ORIGINAL ARTICLE

Strategic Formulation of Dasatinib Nanosponges by Box–Behnken Design for an Improved Oral Delivery

Asfia Kauser, Saritha Chukka

Department of Pharmacy, Chaitanya (Deemed to be University) Pharmacy, Warangal, Telangana, India

Abstract

Introduction: Dasatinib (DAS) a second-generation tyrosine kinase inhibitor has proven to be highly effective in inhibiting the growth of tumors but suffers from low solubility. **Materials and Methods:** The objective of this research was to create innovative nanosponges (NSPs) using hydroxypropyl-β-cyclodextrin (HPβCD) polymer for delivery of DAS a hydrophobic anticancer drug to expand its oral bioavailability using a factorial design approach as a tool for optimization methodology. **Results and Discussion:** Formulation and process variables were optimized for developing NSPs using Design-Expert® software. Particle size, polydispersity index, and percentage entrapment efficiency (EE) were the main focuses of optimization. The techniques used for validation included in vitro release tests, in vivo studies, scanning electron microscopy, differential scanning calorimetry, and Fourier transform infrared spectroscopy. Following optimization, 0.591 molar percentage (P: CL) DAS-loaded HPβCD NSPs were created and agitated for 278 min at 3282 rpm, yielding a desirability of 0.706. The selected formulation showed a size of 148.3 ± 2.64 nm, with polydispersity index of 0.221 ± 0.043, with a zeta potential of −22.5 ± 2.83 and EE of 72.62 ± 3.31%%. The effectiveness of the optimization has been verified by a number of analyses, showing significant increases in area under the curve0-t (8.488-times) and C_{max} (7.355 times) when compared to the free medication. **Conclusion:** From this study, we conclude that using NSPs as a delivery system for DAS has great potential for treating advanced tumors by improving release and bioavailability.

Key words: Box–Behnken design, crosslinker, dasatinib, diphenyl carbonate, hydroxypropyl-β-cyclodextrin, quality by design, Solubility

INTRODUCTION

Dasatinib (DAS) is classified as a second-generation tyrosine kinase inhibitor. This multitarget small molecule drug effectively targets a range of tyrosine kinases that play a crucial role in the growth of tumor cells. Notably, it exhibits high sensitivity toward BCR-ABL, the SRC family, receptor tyrosine kinases such as c-KIT, PDGFR, DDR1, and the TEC family kinases, among several others.[1] DAS, as an initial therapy for chronic myelogenous leukemia, exhibits a 300-fold higher potency compared to imatinib in suppressing BCR/ABL activity.[2]

Recent research findings indicate that the drug possesses the ability to impede the replication, migration, and invasion of cancer cells, while also triggering apoptosis in tumor cells. Notably, it has exhibited remarkable therapeutic efficacy in treating different types of solid tumors.[3] Furthermore, investigations into its potential application for breast cancer treatment have advanced to the stage of clinical trials. DAS plays a crucial role for patients who have built up resistance or are unable to tolerate imatinib, the initial tyrosine kinase inhibitor approved for clinical use in earlier therapies.[4] DAS, a BCS II drug suffers from poor water solubility, its absorption is significantly influenced by pH, it's a weak basic property, having pKa values of 3.1, 6.8, and 10.8. It tends to precipitate in the small intestine but shows improved solubility in an acidic environment. The drug exhibits a relatively short terminal half-life of 3–4 h.[5] Concurrently, DAS is associated with a range of adverse reactions.[6] The DAS's low oral bioavailability (BA), which ranges from 14% to 34%, is another disadvantage.[1] To

Address for correspondence:
Saritha Chukka, Department of Pharmacy, Chaitanya (Deemed to be University) Pharmacy, Warangal, Telangana, India. E-mail: sarithapuligilla28@gmail.com

Received: 26-02-2025
Revised: 11-05-2025
Accepted: 27-05-2025

ensure safe and effective delivery of DAS, a well-designed drug carrier is crucial. This approach has the potential to enhance its therapeutic efficacy while minimizing adverse effects. Addressing the pharmacokinetic (PK) variability and first-pass metabolism of the current formulation is essential.

Nanotechnology plays a vital role in these situations, providing groundbreaking solutions. Colloidal nanocarriers for drug delivery assist in surpassing the constraints of conventional methods.

Researchers have attempted to increase the solubility of DAS, rate of dissolution, and BA. These includes self-nanoemulsifying drug delivery systems,[7] lipid based systems and nanocrystals,[8] and polymeric solid dispersion.[9] While there are advantages to each of these techniques in terms of release management, a notable drawback is the necessity for *in vivo* studies to demonstrate BA enhancement, along with the associated high costs that can pose a barrier to patient access to therapy. In addition, there is a lack of research on how formulation influences drug absorption and intestinal permeability.[10-13]

The objective was to increase DAS BA by controlling distribution to target sites using HPβCD nanosponges (NSPs). To optimize NSPs, factors impacting formulation and process were looked into and further characterized and evaluated.

MATERIALS AND METHODS

DAS was gifted by M/s. Hetero Drugs Ltd., Hyderabad, India. TCI Chemicals provided glutaraldehyde (25% Aqueous Solution), diphenyl carbonate (DPC), and hydroxypropyl-β-cyclodextrin (HPβCD). We purchased the solvents from S.D. Fine Chemicals in Hyderabad. The dialysis membrane was provided by Hi-media Pvt. Ltd. (cut off of M. wt. 12 kDa).

Analyzing phase solubility of DAS

The methodology for solubility analysis followed Higuchi and Connors protocol. In this method, excess drug (DAS) was added to vials containing HPβCD solutions at various concentrations (0-80 mM). The mixtures were then stirred for 72 hours in the dark at 25°C using a magnetic stirrer. After subjecting to cold centrifugation (12,000 rpm) for 30 min, supernatants were suitability diluted and analyzed for concentration of DAS by ultraviolet (UV) spectrophotometer at 322 nm (PerkinElmer Lambda). Plotting DAS concentration (mM) versus HPβCD concentration (mM) produced solubility profiles. Assuming 1:1 formation of complexes between the solubility-phase profile slope and the stability constant (K1:1), equations (2) were utilized to get stability constant.

$$DAS+HP\beta CD \rightleftharpoons ENT+HP\ \ CDcomplex \quad (1)$$

$$Yield\ percentage = \frac{Weight\ of\ Nanosponges}{Total\ solid\ weight} \times 100 \quad (2)$$

DAS0:DAS solubility in water; [DAS.HPβCD complex] designates the amount of thawed in complexing media, [HPβCD] is the quantity of uncomplexed HPβCD in the media.[14]

DAS-HPβCD complex formation

In accordance with the prescribed protocol, DAS-HPβCD composite was created by mixing equal parts of the DAS and complexing agent in methanol and water (1 mL each).[15]

Development of NSPs based on HPβCD

The HPβCD-based NSPs were created by mixing HPβCD with DPC as a cross-linker at the molar concentration of 0.591. With some slight modifications, the ultrasound-assisted approach was used in accordance with earlier protocols.[16] In a 250 mL flask, HPβCD was dispersed in dimethylformamide before DPC was added. In an oil bath, the reaction mixture was refluxed at 90°C until it liquefied. The final product was purified using ethanol-based Soxhlet extraction, after that water cleanse and an overnight drying process at 60°C. For long-term stability, the dried material subsequently finely powdered, combined with water and lyophilized.

To create DAS-HPβCD NSPs, synthesized HPβCD NSPs were first dissolved in double distilled water, and the required amount of drug was added.[13] The resulting mixture was subjected to sonication while being stirred simultaneously. Afterward, it was centrifuged for 10 min at 10,000 rpm to eliminate any unbound drug. The final product underwent freeze-drying to obtain a dry mass, which was then stored in a desiccator for subsequent testing.

Experimental design

Stat-Ease Inc., located in Minneapolis, Minnesota, USA, used Design-Expert computer software version 13.0 to generate nineteen formulas. The following independent variables were used in the 3-factor, 3-level experimental design: The stirring speed (B rpm), the stirring duration (C min), and the molar ratio of P: CL (A). Dependent parameters, including particle size (PS) (X1), polydispersity index (PdI) (X2), zeta potential (ZP) (X3), and entrapment efficiency (EE) (X4), were examined.[13]

High-performance liquid chromatography (HPLC) study

Equipment

The process of chromatographic separation was performed using an undisturbed maintained Inertsil C18 column,

Shimadzu RP-HPLC with UV/Visible indicator. Ammonium acetate buffer (pH 6.4) and acetonitrile are pooled in the mobile phase in a 65:35 v/v ratio. The flow rate was set to 0.7 mL/min in an isocratic mode. Following the addition of 20 µL of samples, the filtrate solutions were measured at 310 nm.[17]

To prepare the 1 mg/mL stock solution, internal standard Imatinib and DAS were weighed. A calibration curve ranging from 5 and 300 ng/mL was then established by means of a secondary stock solution of 100 µg/mL, achieving an r^2 value of 0.996.[18]

The drug was extracted using the protein precipitation approach. By mixing 250 µL of CAN (acetonitrile) with rat plasma of 50 µland vortexing the mixture, the medication was effectively extracted from the plasma. After centrifuging the supernatant for 10 min at 8000 rpm, chromatography was used to examine it at a wavelength of 310 nm.

PS, PdI and ZP

PS and their PdI of the HPβCD NSPs were estimated by means of dynamic light scattered on a Malvern zeta-sizer. The samples were diluted 10 fold before being dispersed in double-distilled water.[18] A Zeta sizer (Malvern) was used to examine the samples at a temperature of 25°C. PS and PdI values were calculated by repeating each measurement 3 times.[19]

EE and yield percentage

Once the drug-loaded NSPs had completely dried, they were weighed. The yield percentage and EE percentage were computed using the following formulas.

$$\%\ Drug\ Entrapment\ efficiency = \frac{Total\ amount\ of\ the\ drug - Free\ drug}{Amount\ of\ drug} \times 100$$

$$Yield\ percentage = \frac{Weight\ of\ Nanosponges}{Total\ solid\ weight} \times 100$$

Topography using scanning electron microscopy (SEM)

The NSP structure was examined using a Quanta FESEM 250 SEM. The samples were mounted on aluminum stubs using carbon tape, gold-coated through ion sputtering, and analyzed at 30 kV with magnifications from 500× to 10,000×.[18]

Fourier transform infrared spectroscopy (FT-IR)

The FT-IR spectrum was noted by means of a PerkinElmer spectrometer. The samples were analyzed over a wave number range of 4000–400 cm^{-1}.[13]

Differential scanning calorimetry (DSC) and X-ray diffraction (XRD)

The drug's properties as well as its interaction with the chemical nature of the excipients were characterized through DSC (DSC-60, Shimadzu, Japan). Approximately 5 mg of the selected samples were sealed in aluminum pans and heated from 50°C to 400°C at 5°C/min in a nitrogen atmosphere. Calibrated with indium and lead, DSC analysis was used for the determination of the melting point and enthalpy of fusion.[13] The XRD was performed for the selected samples (NSPs, physical mixture [PM] and drug) using an X-ray diffractometer, Philips model. Scanning remained done at a rate of 1°2θ/min with an operating voltage (30 kV) and a current setting of 20 mA.[20]

Drug release

The shake flask method assessed drug release from the pure drug (PD) and HPβCD-loaded nanoparticles (NSPs). Each 10 mg sample was sealed in a dialysis membrane and placed in phosphate buffer (pH 6.8) with 1% Triton X-100. The setup was stirred at 37°C, 100 rpm, with periodic sampling and phosphate-buffered saline (PBS) replacement. Filtered samples were analyzed by HPLC at 310 nm. The experiment, conducted in triplicate, applied kinetic models, selecting the one with the highest R^2.[8]

Analyzing for stability of the sample

Stability of the optimized NSP formulation was performed at accelerated conditions in compliance with ICH Q1A (R2) guidelines. The lyophilized samples were stored in glass vials, securely closed with bromobutyl rubber stoppers, and capped with aluminum seals using a crimper. These vials were placed in a humidity chamber kept at 40 ± 2°C and 75 ± 5% RH for 90 days. At predetermined breaks (0, 15 days, 1, 2, and 3 months), key parameters such as physical appearance, PS, ZP, PdI, and EE were evaluated.[19]

Ex vivo permeability studies

With slight amendments, an *ex vivo* study utilizing an inverted intestinal pouch was conducted following previously described methods.[21]

The Institutional Animal Ethics Committee (IAEC)-approved protocol (1447/PO/Re/S/11/CPCSEA-86/A) involved male Wistar rats, randomly allocated to PD and drug-loaded HPβCD NSP groups (n = 3 each). After anesthesia with ether, intestines were excised and purged with ice-cold saline, and a 5 cm ileum segment was isolated. One milliliter of PD or HPβCD NSPs (2.0 mg) was presented into tied sacs, which were then immersed in 40 mL PBS (pH 7.4) for experimentation.[18]

At intervals of 10–120 min, 3 mL samples were taken to measure drug transport from the mucosal (M) to the serosal

(S) side. Drug transfer was analyzed by HPLC at 310 nm, and the apparent permeability coefficient (Papp) was calculated.[14]

$$Papp = dQ/dt + 1/(A+C0) \times 100$$

here dQ/dt represents the drug transportation rate on the serosal side, A denotes the surface area of the gastrointestinal sacs, and C0 is the initial concentration inside the sacs.[18]

In situ single-pass intestinal perfusion (SPIP) technique

The SPIP analysis was conducted following previously established protocols. In summary, the animals were separated into two groups, each consisting of three individuals. One group received PD, while the other was treated with the NSPs preparation. To induce anesthesia, rats were administered thiopental sodium intraperitoneally at a dose of 50 mg/kg. A precise incision of 3–4.5 cm was made along the midline of the abdomen to isolate a nearly 10 cm ileal segment, with the ileocecal junction serving as a distal marker. Both ends of the ileum were excised, and the lumen was rinsed with normal saline at 37°C before being cannulated and protected with silk sutures.

The drug in PBS (pH 7.4) was infused through a syringe pump (1 mL/min, 5 min), followed by continuous perfusion of PD (0.5% sodium carboxymethyl cellulose [CMC]) and drug-loaded HPβCD NSPs (0.2 mL/min, 120 min). To preserve tissue integrity, the intestine was wrapped in isotonic-soaked sterile cotton. Perfusate samples were collected every 10 mins, stored at -80°C, and examined by HPLC. Steady-state outflow concentrations were used to calculate intestinal effective permeability (Peff) through the parallel tube model.

$$Peff,rat = -Q \bullet ln\,(Cout/Cin)/60 \bullet 2\ \ rl$$

Where Q denotes the perfusion flow rate (0.2 mL/min); r represents the radius of the intestinal segment (0.18 cm), and l corresponds to the length of the intestinal section (approximately 10 cm). C_{in} and C_{out} indicate the drug concentration at the inlet and leaving, respectively.[14]

PK studies

Male Wistar rats, averaging 200 ± 20 g in weight and aged 4–5 weeks, were sourced from the ICMR research lab in Telangana, India. The study adhered to the "Guidelines for Care and Use of Laboratory Animals" and was permitted by the IAEC under protocol number 1447/PO/Re/S/11/CPCSEA-86/A. Preceding the experiments, the rats were acclimated for one week in a controlled environment with natural light/dark cycles, a relative humidity (RH) of 40–60%, and a temp of 20 ± 2°C. After acclimatization, the rats were grouped and kept individually in cages. Animals were placed in two groups each having six. The selected drug-loaded NSPs (25 mg/kg body weight) and the PD suspended in sodium carboxymethylcellulose (0.5% w/v) were given by oral direction. Blood samples of 300 µL collected from the retro orbital plexus at specific time points: 0.25, 0.5, 1, 2, 4, 6, 12, and 24 h into sterile ethylenediaminetetraacetic acid-treated tubes. The collected blood specimen subjected to centrifugation (7500 rpm) for 10 min by means of a cold centrifuge. The supernatant (plasma) obtained was analyzed by HPLC.[22]

Data and statistical analysis

Data were analyzed with WinNonlin software and PK parameters remained calculated non-compartmentally. Results were presented as mean ± standard deviation and statistically analyzed by means of GraphPad Prism (version 8.05, GraphPad Software, CA).

RESULTS

Phase solubility studies

From the study, it indicates the creation of a complex in the 1:1 molar proportion (DAS: HPβCD) between drug and complexing agent (slope <1). The calculated apparent stability constant (K1:1) is 246.16 m^{-1}, reflecting a 22-fold enhancement in solubility. This investigation revealed a linear correlation between the amount of HPβCD and the DAS solubility. When administered orally or intravenously, both DAS and HPβCD exhibit a linear decline in concentration, which reduces the likelihood of precipitation.[12]

Preparation of NSPs

NSPs of DAS were synthesized using the procedure of ultrasound-assisted approach, employing HPβCD as the complexing molecules. The structure of HPβCD contains cavities that enable it to encapsulate drugs, resulting in

Table 1: Elements of an experiment design

Code	Independent factors	Levels		
I	Molar proportion (P: CL; mg)	(−1)	(0)	(+1)
II	Stirring speediness (rpm)	(−1)	(0)	(+1)
III	Stirring interval (min)	(−1)	(0)	(+1)
	Replies	**Restraints**		
X1	PS	In the range of 200–250 nm		
X2	PdI	In the range of 0.1–0.4		
X3	ZP	Maximum		
X4	EE	Maximize		

PS: Particle size, PdI: Polydispersity index, ZP: Zeta potential, EE: Entrapment efficiency

the foundation of inclusion complexes. The encapsulation process is facilitated by the ability of HPβCD to form OH bonds with the drug, which allows for effective sequestration of the drug within its hydrophobic core. To ensure stability, the NSPs underwent freeze-drying following their initial synthesis.[13]

Formulation by design model for NSPs

The primary design of DAS-loaded NSPs was to achieve a controlled release with improved drug BA. To achieve this end, a comprehensive quality target product profiles should be considered for formulation development and the same is presented in Table 2.

Experimental design

Nineteen runs were carried out in total and consisted of seven core aspects that are as shown in Table 3. Polynomial models of linear, quadratic, and 2FI components were developed by multiple linear regressions. The coefficients for selecting these models were the adjusted R^2 and predicted R^2 and coefficient of variance.

PS

The results of the initial analysis showed that the mean PS, %EE, ZP, and PdI of drug-loaded HPβCD NSPs were significantly affected through the selected parameters. After analyzing each of these factors separately, ranges were established for the molar proportion (0.4–0.8), stirring speed (250–5000 rpm) and stirring duration (240–420 min). Between different batches, the PS ranged from 122.8 to 448 nm, the PdI from 0.108 to 0.46, the ZP from −33.1 to −11.22, and the percentage of EE from 46.8% to 79.1%. Using the Analysis of Variance (ANOVA) test and the Design-Expert software version 13.0, a quadratic model was fitted to the responses.

The F-value of the model, which stands at 69.99, suggests a mere 0.01% probability that the observed results are attributable to random variation. This supports the classification of the model as "quadratic" and indicates a minimal lack of fit, measured at 2.01. In comparison to pure error, there is a 21.44% likelihood that this lack of fit is not significant. ANOVA analysis revealed that variables with *P*-values under 0.0500 exert a significant impact on the response. The corrected R^2, R^2 and predicted R^2 values were recorded at 0.9851, 0.9701, and 0.8702, respectively. The model demonstrated sufficient precision, achieving a value of 24.719, which exceeds the necessary threshold of 4. All standard interactions (A, C, BC, B^2, C^2) had a significant effect on the results, with *P*-values falling under 0.05.[13] Subsequently, these variables are supposed to be significant, and the regression comparison is as follows:

$$\text{Particle size} = 145.01 - 83.99A - 13.14B + 16.83C - 1.72AB - 4.15AC - 136.85BC - 15.81A^2 + 74.96B^2 + 66.98C^2$$

Surface response (SR) and contour plots (CP) with perturbation roles were used to judge the prime and interaction effects of several factors on size [Figure 1].

Table 2: Selection and rationale of QTPP and CQAs

QTPP	Target	Justification
Preparation	NSPs	NSPs may help in delivering SR (sustain release)
Route of administration	Oral	Marketed formulation meant for oral route and hence we are focusing toward increasing drugs BA.
Dissolution studies	Should be high as compared to plain drug	Long-term release at the intended location may increase the medication's availability.
Pharmacokinetics	Superior compared to the presently available version.	For improved BA
Stability		The effectiveness of the preparation depends on maintaining a consistent PS.
	CQAs	
CQA	**Target**	**Justification**
PS	nm	Decreasing PS to the nanoscale enhances the surface area, thereby improving both dissolution and drug release, which results in greater BA
PdI	<0.3	A PdI of < 0.3 signifies a uniform formulation.
ZP	High	A high value signifies the system's stability.
EE	High	High entrapment contributes to a decrease in the required dosage of the drug

CQA: Critical quality attributes, QTPP: Quality target product profiles, PS: Particle size, PdI: Polydispersity index, ZP: Zeta potential, EE: Entrapment efficiency

Table 3: Runs designed for the trails (DAS dose = 30 mg)

Run	Factor A	Factor B	Factor C	Response 1	Response 2	Response 3	Response 4
	Molar proportion (P: CL)	Stirring speed	Stirring duration	PS	PdI	ZP	EE
1	0.6	3750	330	137.8	0.24	−23.48	72.6
2	0.6	2500	240	164	0.18	−17.4	55.1
3	0.6	5000	420	136.2	0.24	−20.1	46.8
4	0.8	3750	240	124.9	0.11	−33.1	70.6
5	0.4	3750	240	275.8	0.46	−11.9	74.4
6	0.6	3750	330	136.2	0.24	−24.1	73.89
7	0.6	3750	330	164	0.18	−22.4	69.64
8	0.6	3750	330	124.9	0.11	−28.1	72.6
9	0.6	3750	330	134.4	0.2	−27.29	79.1
10	0.6	3750	330	164.4	0.24	−20.63	72.6
11	0.4	2500	330	328.6	0.403	−11.22	62.2
12	0.6	2500	420	448	0.42	−13.1	58.1
13	0.4	3750	420	341.1	0.37	−18.28	57.6
14	0.6	3750	330	153.4	0.26	−23.44	73.6
15	0.8	2500	330	157.4	0.108	−25.2	58.2
16	0.6	5000	240	399.6	0.42	−15.22	75.42
17	0.8	5000	330	139.5	0.2	−25.18	64.9
18	0.4	5000	330	317.6	0.411	−15.2	61.3
19	0.8	3750	420	171.5	0.252	−22.8	65.3

DAS: Dasatinib, PS: Particle size, PdI: Polydispersity index, ZP: Zeta potential, EE: Entrapment efficiency

A two-dimensional perturbation plot comparing predicted and actual results based on selected parameters is displayed in Supplementary Figure 1. The molar ratio of the cross-linker to polymer increased while the PS decreased. A and B have a relatively small effect compared to variable C: stirring speed; stirring time.[23]

PdI

The PdI serves as a dimensionless indicator of the range of distribution of size, stereotypically falling between 0 and 1.[24] A PdI value >0.5 means the particles are heterodisperse or badly distributed. The formulations obtained had a PdI value of between 0.108 and 0.46. The typical F-value of 13.21, which thus indicates a 0s.01% coincidental chance that the results obtained are due only to random variation, and this indicates only a minor lack of fit for the proposed "quadratic" model, but one that is statistically significant. The F-value (0.05) associated with lack of fit indicates that the lack of fit is not statistically significant when accounting for pure error, while the elevated F-value for lack of fit has a 98.48% probability of being attributed to noise.[14] The ANOVA analysis determined some significant variables for consideration, with a *P*-value (< 0.05); hence, the non-significant values were eliminated to improve the replica's precision. The obtained regression coefficients were $R^2 = 0.9296$, adjusted $R^2 = 0.8593$, and predicted $R^2 = 0.8801$. The adequacy of the model for scanning the design space was further confirmed by the existence of an acceptable precision value of 11.5423 greater than the threshold value of 4.

The influence of model terms (A, AC, BC and C^2) was found highly significant at a $P < 0.050$. Hence, it is a significant term, and the corresponding regression equation is given below.

$$PdI = +0.2100 - 0.1218\ A + 0.0200\ B + 0.0140\ C + 0.0210\ AB + 0.0580\ AC - 0.1050\ BC + 0.0268\ A^2 + 0.0438\ B^2 + 0.0612\ C^2$$

Positive values for correlation coefficients indicate that rise in the related variable corresponds to a greater PdI. A negative correlation constant (−0.0155) that it results in a lower PdI. PdI is significantly impacted by the rate of homogenization, as seen by response surface plots [Figure 2]. Although all formulations had PdI values in acceptable ranges below 0.3, reduced molar concentrations and increased stirring rates of the polymer relative to the cross-linker caused a small increase in the PdI value. Even though increased stirring initially promotes monodispersity, too intense agitation introduces additional energy to the particles such that their repulsive interactions are diminished leading to agglomeration. This

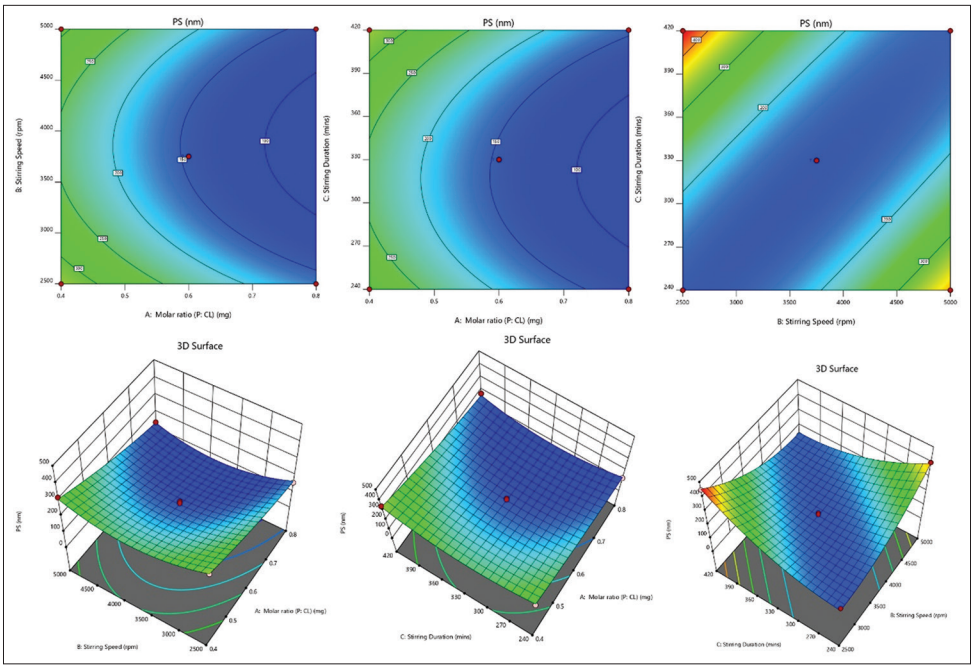

Figure 1: Surface response and contour plots demonstrating variable properties on particle size

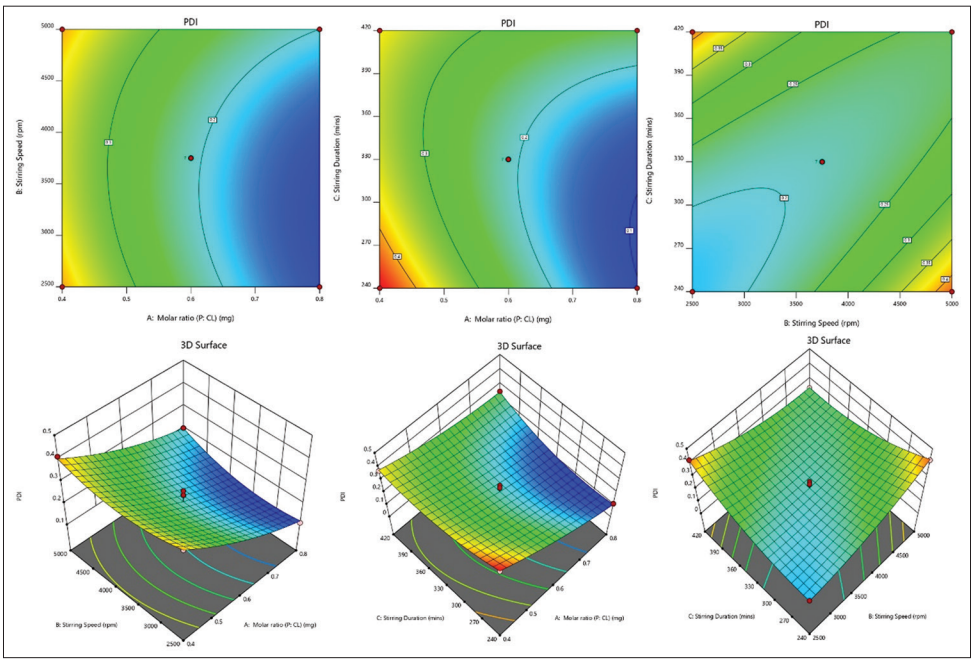

Figure 2: Graphical depiction of response surface, contour plots, and predicted *vs.* actual plots illustrating variable effects on polydispersity index

phenomenon corresponds with the noted augmentation in dimensions that exceed the ideal level of homogenization level.

ZP

Surface charges significantly influence nanoparticle stability and interactions with cell membranes, crucial for drug delivery. The ZP of nanobubbles ranged from −33.1 mV to −11.22 mV. The quadratic model was highly significant (F = 12.99), while the lack of fit (F = 0.04) was insignificant, attributed to pure error. This suggests a high F-value for lack of fit at 0.14, with a 92.99% likelihood of being caused by noise. The regression coefficients, including R2R^2R2, adjusted R2R^2R2, and predicted R2R^2R2, were determined to be 0.9285, 0.8570, and 0.8325, respectively, which therefore had close agreements between predicted and adequate R^2 and varied with just 0.2. The model obtained a signal-to-noise ratio of 13.2279, which is much more than

the required value of 4, meaning that it effectively explored the design space. This implies that A, AC, B^2, and C^2 had a significant impact on ZP since their $P < 0.0500$, thus making them crucial in the regression equation.

$$ZP = -24.21\text{-}6.21\ A - 1.10\ B + 0.4175\ C + 1.0000\ AB + 4.17\ AC - 2.29\ BC - 0.0296\ A^2 + 5.04\ B^2 + 2.72\ C^2$$

ZP increases when the corresponding variable or variables are increased; this is known as a direct relationship and is indicated by positive coefficients. Negative coefficients, on the other hand, indicate an inverse link and suggest that a drop in the relevant variable may lead to drop ZP. Figure 3 displays the surface response and contour plots that demonstrate how the variables affect ZP.

EE

The independent variables affected EE within a range of 46.8% and 79.1% [Figure 4]. The F-value calculated at 23.65 for the model is a means of impressing the significance of the "quadratic" model that showed negligible fitting errors. The model lacked a good fit with an F-value of 0.21, implying an 88.51% probability that the high F-value was caused by random variation. The regression coefficients were 0.9594 for R^2, 0.9189 for adjusted R^2 and 0.8880 for predicted R^2. The model effectively investigated the design space, bolstered by a signal-to-noise ratio of 16.0639, which surpasses the necessary threshold of 4. The variables (C, AC, BC, A^2, B^2, C^2) exhibited *P*-values below 0.0500, signifying their substantial influence and relevance within the regression equation.

$$EE = +73.43 + 0.4375\ A + 1.85\ B - 5.97\ C - 1.90\ AB + 2.88\ AC - 7.91\ BC - 1.83 A^2 - 9.95\ B^2 - 4.63\ C^2$$

A positive correlation implies that an escalation in the associated variable or factors leads to a larger degree of drug entrapment.[25]

Design confirmation

In the validation step, three separate checkpoints were used to test the reliability of the model and the accuracy of the synthesis. The predicted mean values of the EE, ZP, PdI, and size were compared with the experimental mean standards, which were found to be 148.3 ± 2.64 nm, 0.221 ± 0.048, −22.54 ± 2.92, and 76.20 ± 1.41%, respectively. The strong correlation observed between the forecasted and observed outcomes substantiated the model's validity [Figure 5].

PS, ZP, PdI, EE and % yield measurements

The resulting NSPs had homogenous nanosuspension and consistent PSs, with PS ranging from 148.38 ± 2.64 nm to 0.221± 0.043 PdI. A homogenous system is designated by a PdI value <0.3. The improved formulation's ZP measurement, which indicates the surface charge of colloidal particles, was −22.54 ± 2.83 mV, indicating steric stabilization by the stabilizer. Stability of formulation is aided by a higher ZP. For the improved NSPs, the yield percentage was 65.84 ± 3.41 % and the EE was 72.62 ± 3.31%. Optimized NSPs for PS, PdI and ZP of are shown in Figure 6.

SEM

SEM images [Figure 7] illustrate the surface morphology for both the original drug and the amplified NSPs. The untreated drug showed a large-size distribution, which was qualitatively

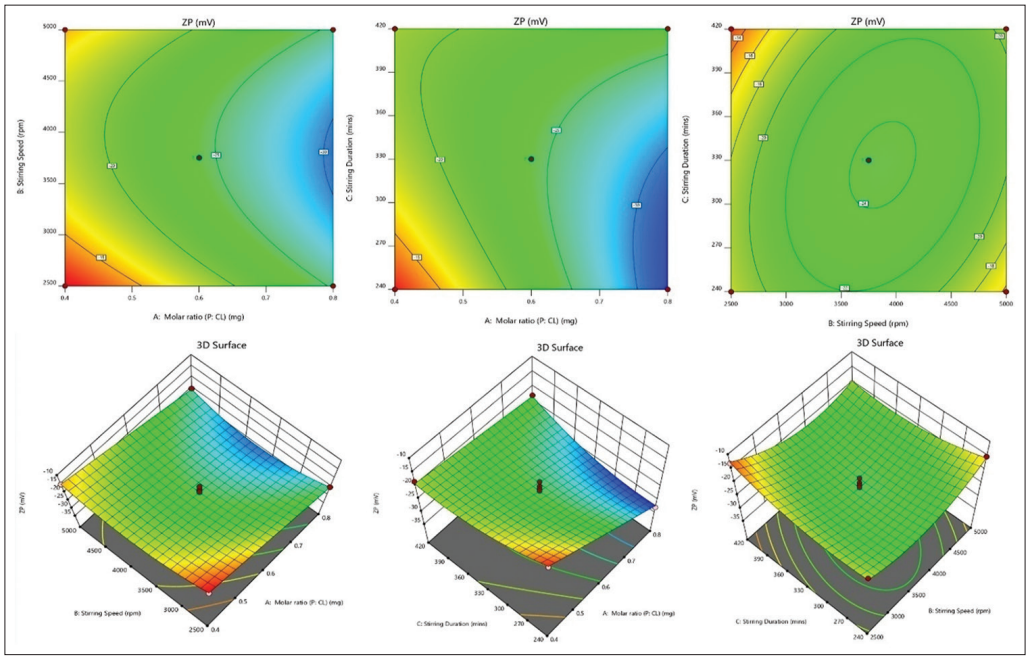

Figure 3: Graphical representation of Surface response and contour plots demonstrating the consequence of factors on zeta potentia

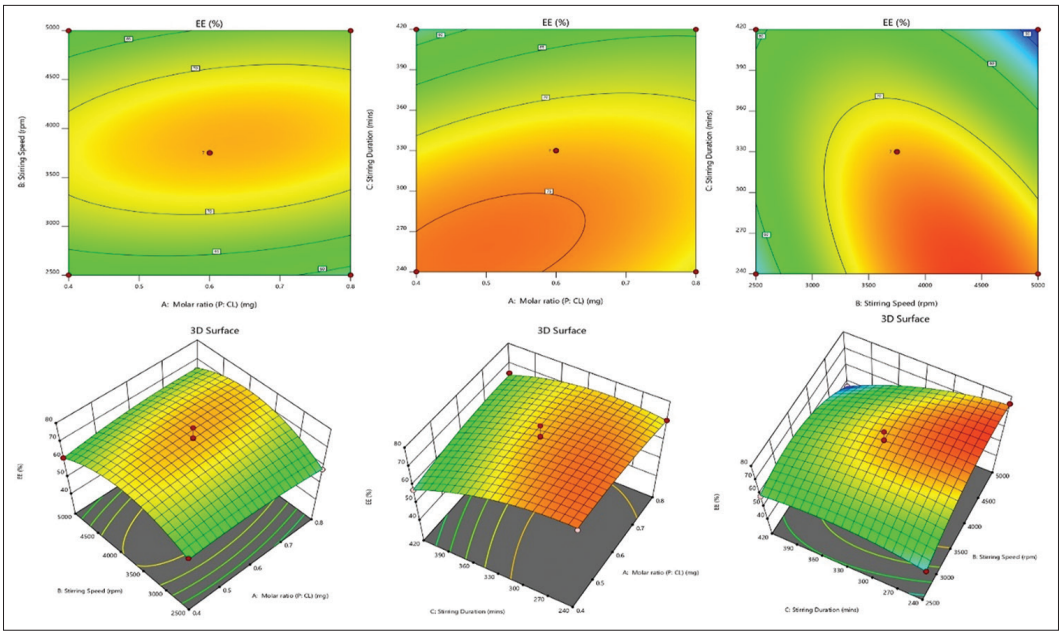

Figure 4: Graphical illustration of surface response and contour plots depicting the impact of selected factors on entrapment efficiency demonstrating the consequence of factors on zeta potential

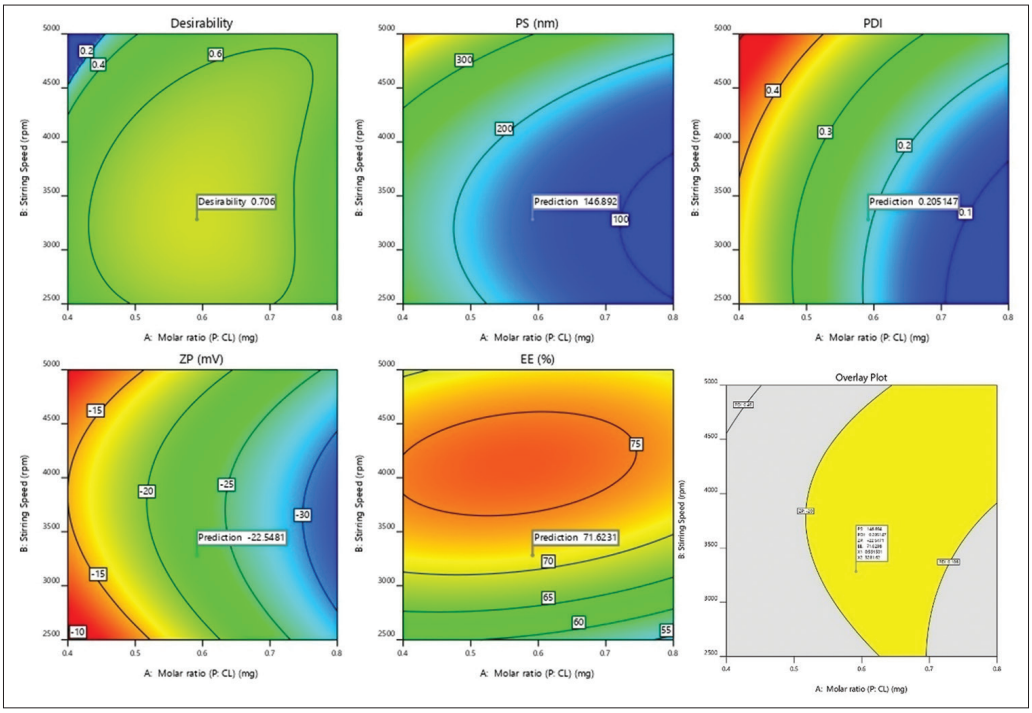

Figure 5: Graphical illustration of desirability plot and overlay pattern

observed as irregular cubic particles on a micron scale. On the other hand, the optimized NSPs transformed the original drug into uniformly spherical NSPs. This visualization indicates that the formulation of NSPs successfully downsizes the drug to a nanodimension size.

FT-IR

The FT-IR spectra are shown in Figure 8. The DAS exhibits distinct peaks in its spectrum, which signify the existence of specific functional groups. Key absorptions include the N–H stretch at 3456.06 cm^{-1}, O–H stretching at 3244.38 cm^{-1}, C–C stretch at 1383.0 cm^{-1}, C=O stretching at 1448.59 cm^{-1}, C–N stretching at 1166.97 cm^{-1}, and aromatic S–H stretching at 1008.80 cm^{-1}).[9] In the case of saccharide vibrations in HPβCD, peaks were observed at about 3343 cm^{-1}, 2924 cm^{-1}, 1645 cm^{-1}, and 1025 cm^{-1}.[26] These peaks are assigned to bending (O–H), stretching (C–O), as well O–H, and C–H stretch, correspondingly.[13] A peak at 851 cm^{-1} is the characteristic peak of an α-type glycosidic bond, indicating that the glucopyranose

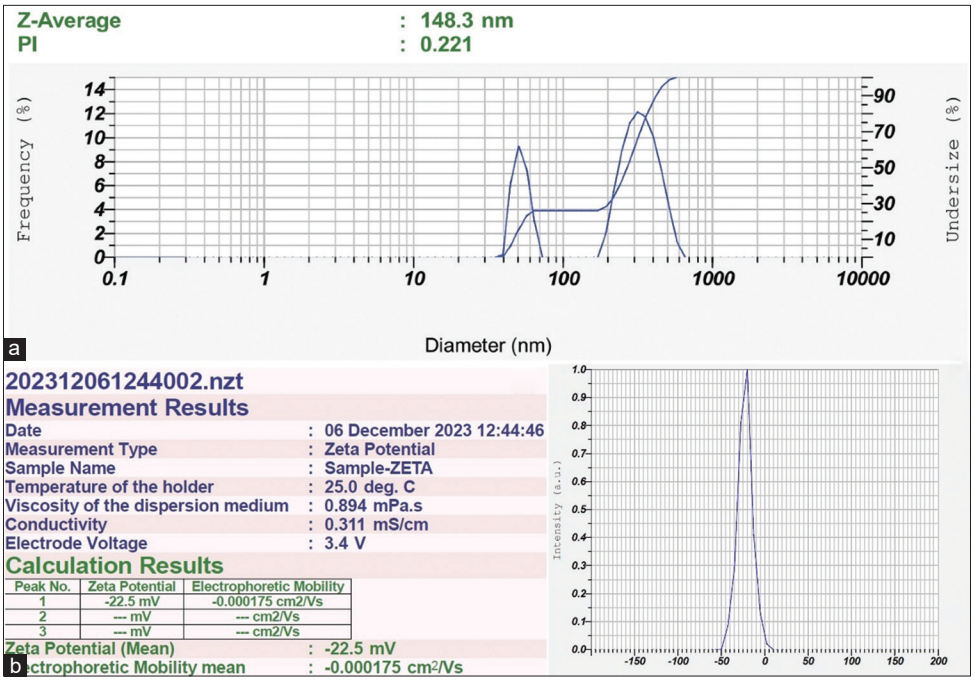

Figure 6: (a) Particle size, polydispersity index of nanosponges (NSPs); (b) Zeta potential of the NSPs

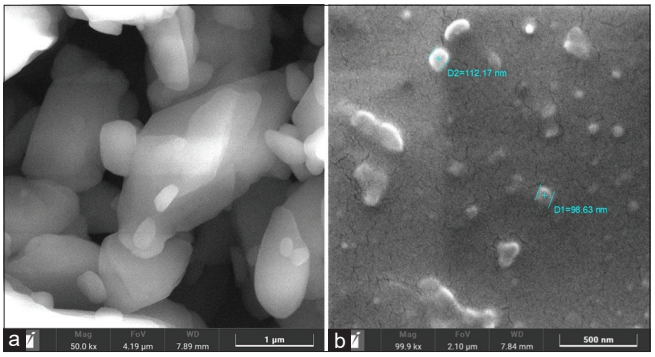

Figure 7: (a) Scanning electron microscopy (SEM) image of pure drug (b) SEM image of the optimized nanosponges

components are associated through α-1,4-glycosidic linkages. The points appearing at a wave number of 2965 cm^{-1} and 1365 cm^{-1} correspond to the anti-symmetric trembling and the CH peak of OH-propyl characteristic peak from complexing agent.[13] The physical mixture spectrum of DAS and HPβCD showed an overlapping of their peaks, and this indicated unique peaks by both components. Importantly, the characteristic peaks of DAS were masked within the nanosponge spectrum, implying potential bond reinforcement due to interactions between DAS and the nanosponge. Moreover, the drug-loaded complex's O-H stretch vibration moved toward larger wavenumbers, indicating the potential development of OH bonds between the drug and complexing agent.

DSC and XRD

Figure 9a and b represent the DSC and XRD patterns. The melting endotherm of PD started at 249.82°C and peaked at

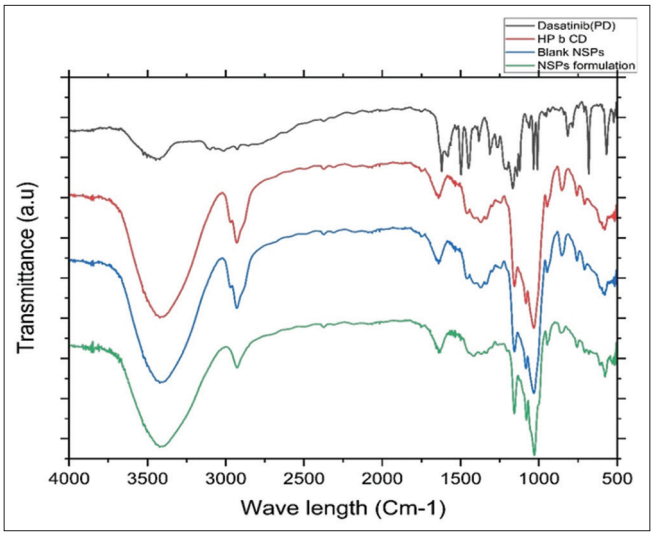

Figure 8: Fourier transform infrared spectroscopy overlay: (a) Drug-pure drug (black color-line); (b) Blanks nanosponges (NSPs) (Blue color-line); (c) β-cyclodextrin (Red color-line); and (d) NSPs-NSPs (Green color-line)

252.4°C and ended at 254.49°C. On the other hand, HPβCD presents a clear-cut melting profile, which starts at 251.11°C, peaks at 242.01°C, and ends at 277.98°C. The drug exhibited more pronounced peaks in comparison to NSPs, possibly because the inclusion complexes were formed between the drug and HPβCD. However, the diffraction melting peak of the drug is absent in the NSPs formulation, while the HPβCD melting peak appears at 232.3°C, suggesting that the drug has undergone solid-state complexation at a molecular level within the NSPs.

Drug release

The drug release profiles are presented in Figure 10 for the PD, drug-loaded simple inclusion complex, and DAS-loaded HPβCD NSPs, over a specified duration. The DAS/HPβCD complexes demonstrate a significant initial burst release, with more than 92.62 ± 8.18% of the drug being released within the first 120 min. In contrast, the optimized HPβCD NSPs show a prolonged release, achieving 95.42 ± 7.16% over a period of 60 h, while the release of the plain drug is limited to only 30.66 ± 6.24%. The Korsmeyer-Peppas (R^2 0.9409) and Higuchi (0.9552) representative indicate high relationships, while the reduced R^2 for the 0 and 1st order (0.770 and 0.444) representations indicate mechanisms of persistent rate and exponential decline in release, correspondingly.

Stability analysis

To assess the stability of the formulation, researchers evaluated physical characteristics, ZP, PS, PDI, and EE throughout a 3-month period [Table 4]. In addition, *in vitro* drug release experiments were conducted at the beginning and end of 90 days. Visual inspection of the lyophilized NSPs revealed no substantial changes in their appearance after 3 months of storage. Encapsulation efficiency also remained consistent throughout the period. However, ZP exhibited a slight decrease, while PS and PdI displayed a minor increase. It is suggested that the potential aggregation of smaller NSPs into larger ones during storage.

After thorough mixing, the NSPs achieved optimal PS, PDI, and ZP, indicating a well-defined and stable formulation. The

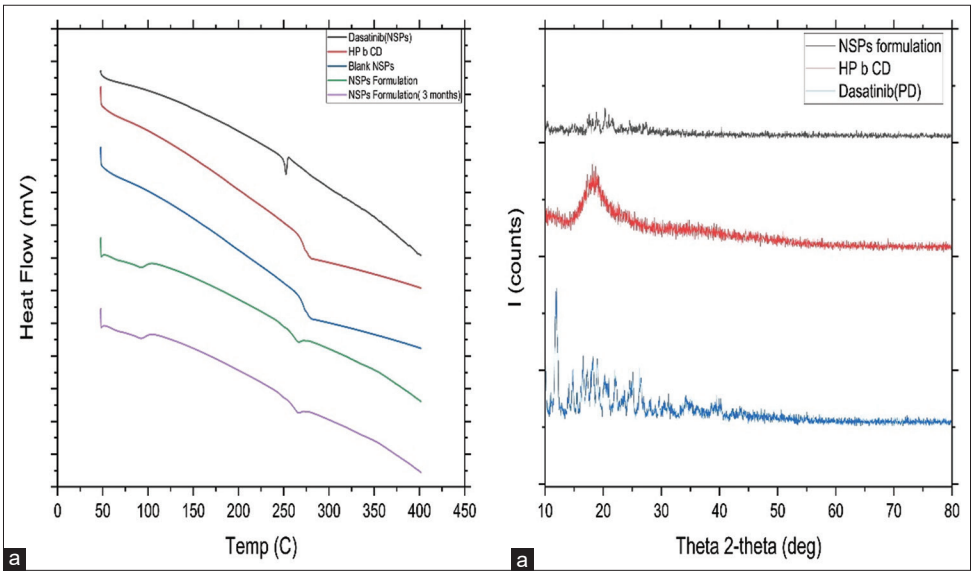

Figure 9: (a) An overlay of differential scanning calorimetry: Pure drug-dasatinib (black color); β-cyclodextrin (β-CD) (red color); Blank nanosponges (NSPs) (blue color); NSPs (green color); and NSPs stored for 3 months (purple color). (b) Overlay of X-ray diffraction: pure drug (blue color); β-CD (red color); and NSPs (black color)

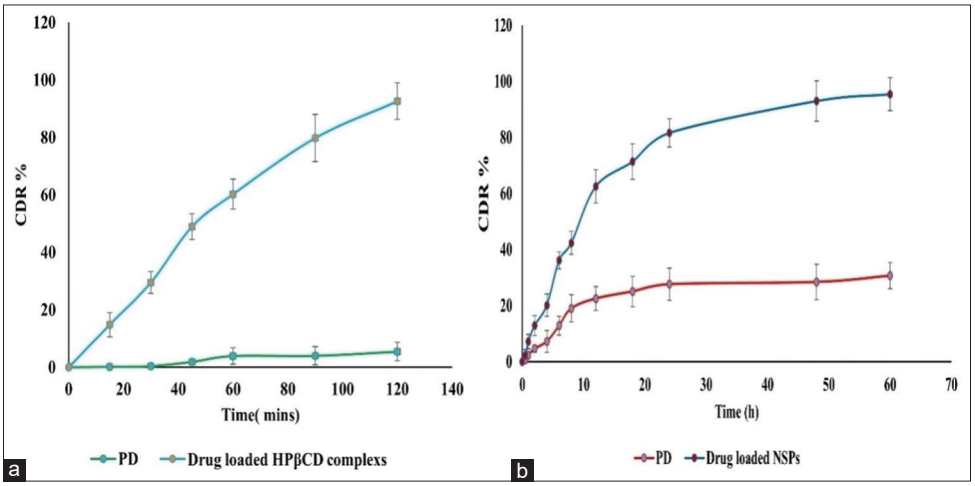

Figure 10: *In vitro* release profiles: (a) Dasatinib (DAS) (pure drug [PD]); DAS-hydroxypropyl-β-cyclodextrin complex; (b) DAS (PD), DAS-nanosponges

Table 4: Parameters that are assessed during accelerated stability studies

Evaluation parameters	At 0 days	At 90 days
Physical appearance	NSPs were fluffy with uniform texture	NSPs were fluffy and with uniform texture
PS (nm)	148.3±2.64	150.3±3.3
PdI	0.221±0.043	0.229±0.049
ZP (mV)	−22.5±2.83	−24.8±3.63
EE (%)	72.62±3.31%	70.81±3.90%
CDR (%) at 60 h	95.42±7.16	94.33±8.02

NSPs: Nanosponges, PS: Particle size, PdI: Polydispersity index, ZP: Zeta potential, EE: Entrapment efficiency, CDR: Cumulative drug release

in vitro drug release profile demonstrated a consistent and uniform drug release from the NSPs throughout the study. Notably, there were no signs of degradation or alterations in the initial release pattern. A comprehensive evaluation of NSPs confirmed the stability of the PB-loaded NSPs even under accelerated storage conditions.

Ex vivo permeability studies

Table 5 presents the mean apparent permeability (Papp) values for PD and DAS-loaded HPβCD NSPs. The formulation outperformed the PD, enhancing Papp by 2.331-, 1.854-, and 2.75-fold in the duodenum, jejunum, and ileum, respectively, indicating improved mucosal permeability.[14] DAS-loaded HPβCD NSPs showed higher permeability in the duodenum and ileum, likely due to transporter expression differences. NSPs may alter drug ionization and protect uptake transporters, enhancing absorption through transporter-mediated mechanisms.

In situ SPIP technique

Despite showing promising results in laboratory studies, many drugs face challenges when administered to animals or humans, such as poor absorption, water insolubility, and unstable physical properties. The gut mucosa serves as a significant barrier and is a primary contributor to these issues. To assess the *in vivo* effectiveness of the formulation, we employed perfusion techniques to evaluate the permeability of the PD and DAS-loaded HPβCD NSPs in the rat ileum.[14]

Effective permeability (Peff) increased significantly from 0.082×10^{-4} to 0.49×10^{-4} cm/s. The *in situ* SPIP method, which simulates physiological conditions, demonstrated enhanced intestinal permeability with NSP-based delivery. This improvement is linked to smaller PS, greater surface area, better dissolution, and higher solubility, making NSPs promising for predicting human drug absorption.

PK

Table 6, Figure 11 and 12 illustrates the plasma concentration-time profile of the drug following oral administration of the standard pharmacodynamic solution (0.25% w/v sodium CMC) and the optimized NSPs.

Table 5: Mean apparent permeability of PD and DAS β-CD NSPs

Colonic section	PD (Papp, * 10^{-4} cm/s)	DAS HPβCD NSPs (Papp, * 10^{-4} cm/s)
Duodenum	0.36	0.86
Ileum	0.49	0.91
Jejunum	0.39	0.98

PD: Pure drug, DAS: Dasatinib, NSPs: Nanosponges, HPβCD: Hydroxypropyl-β-cyclodextrin

Table 6: PK parameters

PK parameters	PD	Drug-loaded NSPs
C_{max} (ng/mL)	202.153±48.22	1487.052±67.62
T_{max} (h)	2.5	2.5
Half-life (h)	2.564±0.34	3.608±0.49
AUC_{0-t} (ng. h/mL)	780.94±84.18	6629.05±502.6
$AUC_{0-in}f$ (ng. h/mL)	818.605±112.06	7080.26±480.04
Ke (h^{-1})	0.270	0.192
MRT	4.284	6.697

PK: Pharmacokinetic, AUC: Area under the curve, NSPs: Nanosponges, PD: Pure drug, MRT: Mean residence time

NSP formulation compared to the PD suspension showed suggestively a relatively high T_{max}, C_{max} (**$P < 0.001$), area under the curve $(AUC)_{0-24}$ (**$P < 0.001$), and $AUC_{0-\infty}$ (**$P < 0.001$). Figure 12 indicates that AUC for DAS NSPs formulation was considerably higher compared to the PD.[13]

The formulation of NSPs exhibited a significantly greater maximum concentration (C_{max}) at a rate of 7.355-fold and an AUC_{0-t} at 8.488-fold when compared to the free drug. This formulation is characterized by sustained release properties, which facilitate prolonged retention and improved BA. In addition, the DAS-loaded NSPs demonstrated a longer half-life in comparison to the PD suspension, further supporting the sustained release effect. The incorporation of NSP carriers

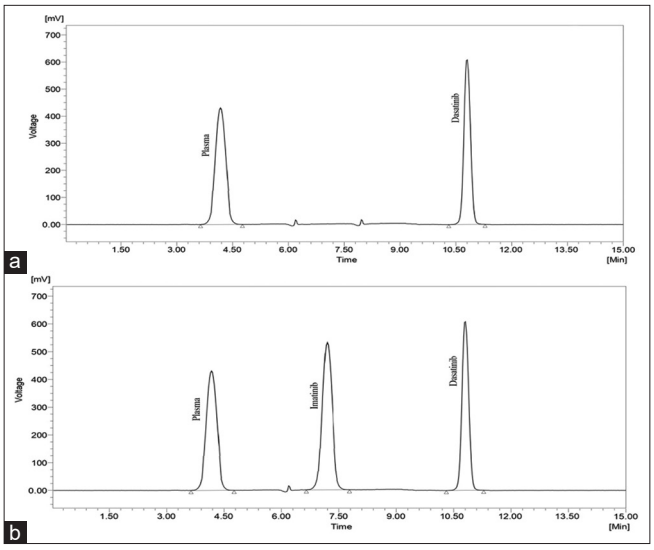

Figure 11: Bioanalytical chromatogram drug in plasma (a) and internal standard and drug in plasma (b)

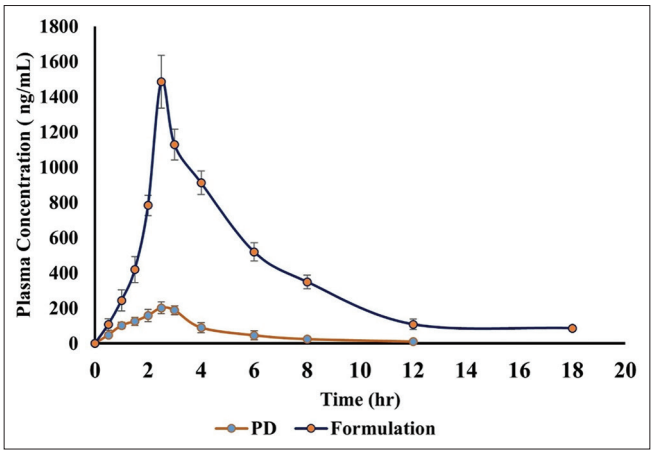

Figure 12: *In vivo* pharmacokinetic studies

significantly enhances drug solubility and release, resulting in substantial improvements in PK profiles.

DISCUSSION

In this research, we formulated and developed DAS-loaded HPβCD NSPs through an ultrasound-assisted method. The phase analysis was evaluated using the Higuchi-Connors approach, revealing the establishment of type AL complexes among DAS and HPβCD.[11]

Cyclodextrins markedly enhance the water solubility of DAS. Interaction of HPβCD with DAS significantly enhances its solubility, especially at saturated concentration of about 40 mM of HPβCD. NSPs were stabilized through the hydrophobic interaction between the drug and HPβCD, but HPβCD's hydrophilic surface could help distribute NSPs in the water. This increased solubility and stability extend the pharmaceutical applications of DAS. The application of the Box–Behnken design resulted in the development of a linear model to study significant parameters such as PS, PdI, ZP, and EE. The presence of positive coefficients suggests that an increase in the relevant variables is associated with enhanced EE. Both elevated and reduced concentrations of the stabilizer resulted in a bit larger particles, due to the uncontrolled diffusion of nuclei at lower concentrations. Although PdI values stayed within the acceptable limit (<0.3), higher stirring rates resulted in slightly higher PdI due to the increased energy of particles, which reduced the repulsive forces and resulted in agglomeration instead of ideal conditions for homogenization. FTIR analysis confirmed the efficient encapsulation of DAS in HPβCD NSPs and also reflected an increased interaction between the two species. The shifts in the N-H and O-H stretching vibrations toward higher wavenumber values for the DAS-HPβCD complex indicate the establishment of hydrogen bonding among the drug and HPβCD.[11] This coinciding melting point of the drug-cyclodextrin mixture, therefore, signals a significant interaction between the drug and cyclodextrin. Even with optimized HPβCD NSPs, drug encapsulation into cyclodextrin strengthens its thermal stability. The Kelvin outcome indicates that smaller, free particles soften at lesser temperatures than larger bulk forms. However, although HPβCD inclusion NSPS forms spherical aggregates and various solid-state configurations, they do not demonstrate porous structure.[27] The SEM images indicate that these molecules aggregate into distinct spherical shapes characterized by noticeable porosity. The incorporation of DAS into HPβCD alters its crystalline structure, as shown by the diminished intensity of the XRD peaks. This suggests that the drug is either dispersed or converted into an amorphous form within the HPβCD matrix, leading to a reduction in the overall crystallinity of the sample. The effective encapsulation within HPβCD NSPs leads to the creation of inclusion complexes, which is evidenced by the lower intensity of the XRD peaks. The observed burst release pattern from these complexes aligns with findings from prior research, indicating that the drug is easily released through mechanisms such as dilution or competitive complexation.[28] Liberation of DAS from NSPs occurs in a uniform manner without any burst phenomenon, pointing out that loosely bound or free DAS molecules are absent on the surface of HPβCD NSPs. The sustained release can be attributed to the porous nature of the HPβCD NSPs, which allows stable complexation with DAS and, thus, restricts its fast release.[28] The addition of DPC into the HPβCD framework improves the capability of cyclodextrins to form inclusion complexes with guest fragments by promoting control release through strong binding or gradual dissociation. It has thus been considered to potentially become very effective in handling cancer.[13] The regression coefficients indicate that the drug release mechanism is characterized by a blend of diffusion, as outlined by the Higuchi model, and anomalous transport, as represented by the Korsmeyer–Peppas model. This suggests that the release of the drug is affected by matrix

diffusion along with additional processes such ass polymer relaxation, swelling, or erosion.[29]

The AUC of plasma NSPs containing DAS was highly compared to that of the PD solution. HPβCD NSPs possessed profiles that are favorable for sustained release; thus, prolonged retention and hence enhanced BA ensued. In addition, sustained release is justified by the increased half-life studied in DAS-containing HPβCD NSPs in relation to the pure suspension solution of the drug.[30] The PD suspension achieved its peak plasma concentration (C_{max}) at a faster rate compared to the optimized NSPs formulation. The NSP carriers facilitate increased solubility and drug release, resulting in notable enhancements in PK profiles.

CONCLUSION

DAS-loaded DPC-crosslinked HPβCD NSPs were developed with the objective of improving low BA and poor sustained release of DAS in the cancer treatment. Optimized parameters of the formulation helped HPβCD NSPs attain desired properties, such as size, PdI, ZP, and EE that are considered significant for any drug delivery system. In this respect, the optimized NSPs exhibited *in vitro* sustained release of DAS along with enhanced *in vivo* BA. The porous nanoscale architecture of HPβCD NSPs facilitates sustained drug delivery, thus attaining a more therapeutic effect and increased efficacy as compared to the plain drug. The results indicate HPβCD NSPs as a promising tool in the delivery of oncological drugs; they will result in maximal bioavailability along with providing sustained release for better therapeutic outcomes.

AUTHORS' CONTRIBUTIONS

All the authors equally contributed for the writing of the manuscript.

REFERENCES

1. Lindauer M, Hochhaus A. Dasatinib. Recent Results Cancer Res 2018;212:29-68.
2. Levêque D, Becker G, Bilger K, Natarajan-Amé S. Clinical pharmacokinetics and pharmacodynamics of dasatinib. Clin Pharmacokinet 2020;59:849-62.
3. Talpaz M, Shah NP, Kantarjian H, Donato N, Nicoll J, Paquette R, *et al*. Dasatinib in imatinib-resistant Philadelphia chromosome-positive leukemias. N Engl J Med 2006;354:2531-41.
4. Keating GM. Dasatinib: A review in chronic myeloid leukaemia and Ph+ acute lymphoblastic leukaemia. Drugs 2017;77:85-96.
5. Hořínková J, Šíma M, Slanař O. Pharmacokinetics of dasatinib. Prague Med Rep 2019;120:52-63.
6. Niza E, Nieto-Jiménez C, Noblejas-López MD, Bravo I, Castro-Osma JA, De la Cruz-Martínez F, *et al*. Poly(cyclohexene phthalate) nanoparticles for controlled dasatinib delivery in breast cancer therapy. Nanomaterials (Basel) 2019;9:1208.
7. Rajinikanth C, Kathiresan K. Development and optimization of super saturable self-nano emulsifying drug delivery system for dasatinib by design of experiment. Int J Appl Pharm 2024;16:195-205.
8. Wang C, Wang M, Chen P, Wang J, Le Y. Dasatinib nanoemulsion and nanocrystal for enhanced oral drug delivery. Pharmaceutics 2022;14:197.
9. Sokač K, Milološa M, Kučić Grgić D, Žižek K. Polymeric amorphous solid dispersions of dasatinib: Formulation and ecotoxicological assessment. Pharmaceutics 2024;16:551.
10. Tippareddy A, Marabathuni VJ, Narapusetty N. Dasatinib nasosponges-formulation development and evaluation. J Innov Appl Pharm Sci 2022;7:10-7.
11. Utzeri G, Matias PM, Murtinho D, Valente AJ. Cyclodextrin-based nanosponges: Overview and opportunities. Front Chem 2022;10:859406.
12. Alghaith AF, Mahrous GM, Zidan DE, Alhakamy NA, Alamoudi AJ, Radwan AA. Preparation, characterization, dissolution, and permeation of flibanserin - 2-HP-β-cyclodextrin inclusion complexes. Saudi Pharm J 2021;29:963-75.
13. Reddy KS, Bhikshapathi D. Design and optimization of DPC-crosslinked HPβCD nanosponges for entrectinib oral delivery: Formulation, characterization, and pharmacokinetic studies. Future J Pharm Sci 2024;10:1-15.
14. Sampathi S, Prajapati S, Junnuthula V, Dyawanapelly S. Pharmacokinetics and anti-diabetic studies of gliclazide nanosuspension. Pharmaceutics 2022;14:1947.
15. Durk MR, Jones NS, Liu J, Nagapudi K, Mao C, Plise EG, *et al*. Understanding the effect of hydroxypropyl-β-cyclodextrin on fenebrutinib absorption in an itraconazole-fenebrutinib drug-drug interaction study. Clin Pharmacol Ther 2020;108:1224-32.
16. Dhakar NK, Caldera F, Bessone F, Cecone C, Rubin Pedrazzo A, Cavalli R, *et al*. Evaluation of solubility enhancement, antioxidant activity, and cytotoxicity studies of kynurenic acid loaded cyclodextrin nanosponge. Carbohydr Polym 2019;224:115168.
17. Chokshi A, Gajjar A, Bhanushali P, Desai P. Quantification of antileukemic drug dasatinib in human plasma: Application of a sensitive liquid chromatographic method. J Chem Metrol 2021;15:152-62.
18. Gera S, Talluri S, Rangaraj N, Sampathi S. Formulation and evaluation of naringenin nanosuspensions for bioavailability enhancement. AAPS PharmSciTech 2017;18:3151-62.
19. Aldawsari MF, Alhowail AH, Anwer MK, Ahmed MM. Development of diphenyl carbonate-crosslinked cyclodextrin based nanosponges for oral delivery of baricitinib: Formulation, characterization and

pharmacokinetic studies. Int J Nanomedicine 2023;18:2239-51.
20. Moin A, Roohi NK, Rizvi SM, Ashraf SA, Siddiqui AJ, Patel M, *et al*. Design and formulation of polymeric nanosponge tablets with enhanced solubility for combination therapy. RSC Adv 2020;10:34869-84.
21. Neerati P, Kumar Bedada S. Effect of diosmin on the intestinal absorption and pharmacokinetics of fexofenadine in rats. Pharmacol Rep 2015;67:339-44.
22. Arumugam AO, Abbott HC. An open-label, balanced, randomized, two treatments, two sequences, four periods, fully replicate, crossover study to evaluate the bioequivalence of Dasatinib 100 mg film-coated tablets of Abbott Laboratories versus Sprycel® (Dasatinib) 100 mg film-coated. JSM Bioavail Bioequiv 2022;2:1007.
23. Palanati M, Bhikshapathi DV. Development, characterization and evaluation of entrectinib nanosponges loaded tablets for oral delivery. Int J Appl Pharm 2023;15:269-81.
24. Danaei M, Dehghankhold M, Ataei S, Hasanzadeh Davarani F, Javanmard R, Dokhani A, *et al*. Impact of particle size and polydispersity index on the clinical applications of lipidic nanocarrier systems. Pharmaceutics 2018;10:57.
25. Rangaraj N, Pailla SR, Chowta P, Sampathi S. Fabrication of ibrutinib nanosuspension by quality by design approach: Intended for enhanced oral bioavailability and diminished fast fed variability. AAPS PharmSciTech 2019;20:326.
26. Yuan C, Liu B, Liu H. Characterization of hydroxypropyl-β-cyclodextrins with different substitution patterns via FTIR, GC-MS, and TG-DTA. Carbohydr Polym 2015;118:36-40.
27. Peimanfard S, Zarrabi A, Trotta F, Matencio A, Cecone C, Caldera F. Developing novel hydroxypropyl-β-cyclodextrin-based nanosponges as carriers for anticancer hydrophobic agents: Overcoming limitations of host-guest complexes in a comparative evaluation. Pharmaceutics 2022;14:1059.
28. Loftsson T. Cyclodextrins in parenteral formulations. J Pharm Sci 2021;110:654-64.
29. Argenziano M, Gigliotti CL, Clemente N, Boggio E, Ferrara B, Trotta F, Dianzani C. Improvement in the anti-tumor efficacy of doxorubicin nanosponges in *in vitro* and in mice bearing breast tumor models. Cancers (Basel) 2020;12:162.
30. Zidan MF, Ibrahim HM, Afouna MI, Ibrahim EA. *In vitro* and *in vivo* evaluation of cyclodextrin-based nanosponges for enhancing oral bioavailability of atorvastatin calcium. Drug Dev Ind Pharm 2018;44:1243-53.

Source of Support: Nil. **Conflicts of Interest:** None declared.

SUPPLEMENTARY

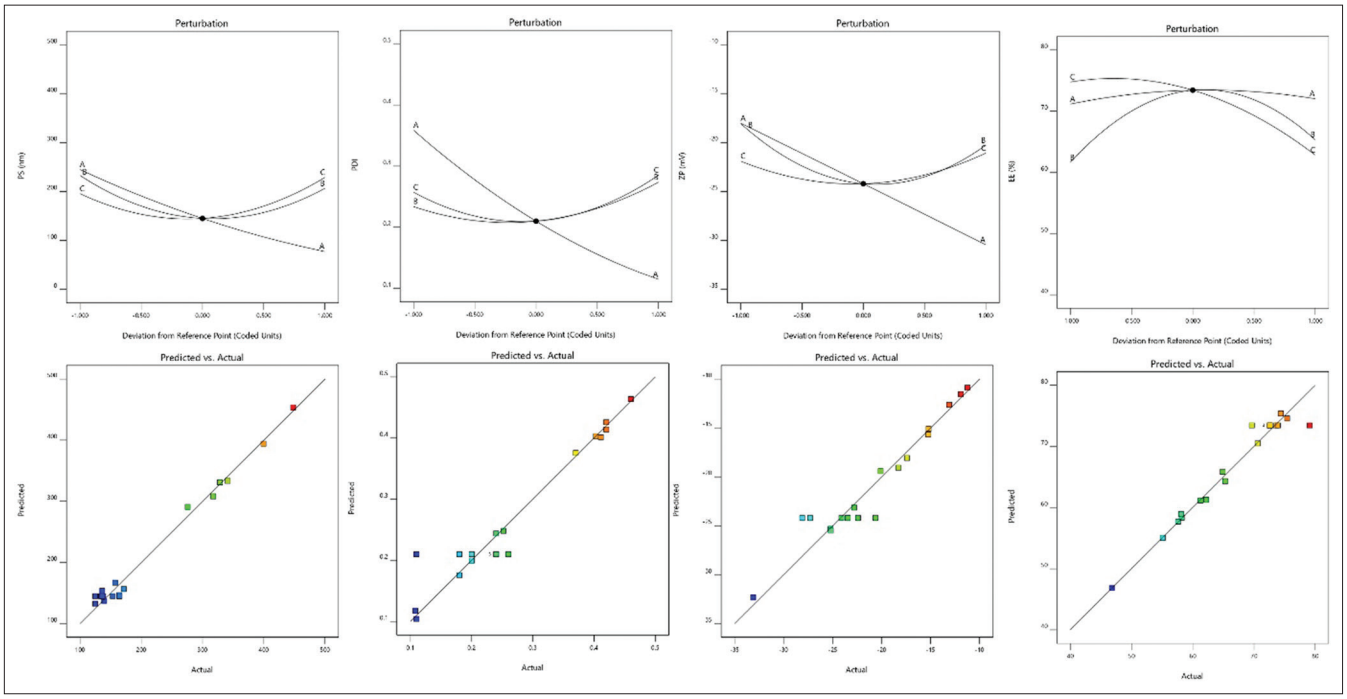

Supplementary Figure 1: Two-dimensional perturbation plot showing the influence of molar